Evolution of Electrosprayed Particles at a Static Air-Water Interface on Multiple Time Scales

Joseph M. Prisaznuk[1], Xin Yong[2†], and Paul R. Chiarot[1*]

[1]Department of Mechanical Engineering, State University of New York at Binghamton, Binghamton, NY 13902, USA

[2]Department of Mechanical and Aerospace Engineering, University at Buffalo, Buffalo, NY 14260, USA

Abstract

Hypothesis

Electrospray deposition offers a field-driven method for efficiently delivering charged nano/microparticles to fluid interfaces with minimal disturbance. At an air-water interface, the long-term arrangement and mobility of colloidal particles is expected to depend on electrostatic repulsion, particle composition, and environmental factors such as ionic strength and surface contamination. These competing effects may give rise to time-dependent transitions that are not accessible in quasi-equilibrium systems.

Experiments

We created a custom fluidic device to generate geometrically stable air-water interfaces via continuous liquid infusion and image-based feedback control. Combined with electrospray interfacial targeting, this platform enabled sustained observation of charged colloidal assembly and dynamics at a fluid interface under non-equilibrium conditions. Particle motion was captured over several hours, and the salt concentration in the aqueous subphase was modulated to establish the different assembly structure regimes.

Findings

Interfacial order progressively degrades over time (> 5 hours) due to charge relaxation, a process that is further accelerated by external ionization. Counterintuitively, adding salt to the subphase enhances hexagonal ordering immediately after deposition, revealing a nontrivial interplay between electrostatic screening and interfacial structure. At intermediate time scales (2-3 hours), we observe spatially heterogeneous diffusion among neighboring particles, which is attributed to localized surface contamination. These results reveal how evolving electrostatic charge drives interfacial self-assembly and long-term colloidal dynamics at liquid interfaces.

Keywords: electrospray, air-water interface, colloid, self-assembly, surface charge, salt, anomalous diffusion

† email: xinyong@buffalo.edu

* email: pchiarot@binghamton.edu

1. Introduction

Colloidal materials form two-dimensional assemblies that underpin many natural phenomena, and have been studied for their potential use as nanoscale building blocks.[1,2] Fluid interfaces provide a versatile platform for colloidal self-assembly, as the liquid-vapor phases allow for reconfigurability[3] and enable the study of non-equilibrium behavior and emergent order in soft matter systems.[4] These interfacial colloidal systems reveal complex collective behavior inaccessible in bulk phases, making them ideal for probing fundamental interfacial phenomena. This is exemplified by the pioneering work in the late 20th century for quasi-2D systems, and more recently to study 3D binary crystal structures.[5,6]

There are numerous forces which govern the assembly of colloids at an interface.[7] Interfacial tension keeps colloidal particles, as well as amphiphilic surface-active molecules, adsorbed to the fluid interface. Once trapped, the arrangement of particles is determined by interparticle forces. Electrostatic forces may arise from surface functionalization of particles or external fields, with like charges leading to repulsion.[8,9] Capillary interactions also play a significant role: the contact angle and wetting behavior of colloids is generally dictated by the particle shape and composition, with capillary attraction for like-shaped menisci.[10] Increased surface roughness of solid particles typically leads to stronger capillary interactions due to the deformation of the interface, while porous particles have exhibited a lower interaction energy due to capillary imbibition.[11,12] Beyond these interparticle forces, the geometry of a liquid-vapor interface may impact the assembly of mesoscale colloidal assemblies.[13] Spatially-varying interfacial curvature can lead to structural changes in the crystalline arrangement of colloids.[14,15]

Early work on interfacial colloidal assembly in the late 1990s and early 2000s established foundational understanding using both air-water and oil-water systems. Investigations of air-water systems considered the adsorption of polymer microparticles to an interface over time as a function of electrolyte concentration.[16,17] However, these experiments were done in dilute systems and did not have sufficient spatial or temporal resolution to consider the interactions between single particles and aggregates over extended periods. Studies of oil-water systems during this period provided clearer insights into interparticle forces. For example, Aveyard et al. measured long-range repulsive forces between charged particles at oil-water interfaces,[18] and Horozov et. al. found that hydrophobic silica particles at an octane-water interface primarily interacted through electrostatic repulsion, resulting from charge present at the particle-octane surface.[19] More recent

studies have confirmed these early results and expanded upon the previous findings, showing that electrostatic dipole-dipole repulsion is a valid theoretical model for particle interactions under many experimental conditions. Parolini et. al. found that the interaction between polystyrene (PS) particles at a water-decane interface can be modeled as a repulsive dipole potential across a wide range of interfacial densities.[20]

Many studies of interfacial colloidal interactions take place at dynamic, evolving interfaces due to evaporation.[21–25] For systems with relatively slow evaporation rates, it is generally assumed that the assembly is in a quasi-equilibrium state. However, this equilibrium may be disturbed by various external forces and cannot always be controlled directly. For example, Marangoni flows due to small amounts of surfactant contamination can disrupt the desired outcome of ordered self-assembly at an interface.[26,27] This is especially true for aqueous systems, as surfactants are readily absorbed from the environment; even small amounts of oil from needles or syringes may introduce defects in the interfacial assembly.[28] Furthermore, at millimeter length scales, evaporation of water becomes significant and introduces time-dependent changes in interface geometry. Passive evaporation control through interfacial self-assembly has been demonstrated,[29] but active compensation for evaporation remains largely unexplored.

Here, we use electrospray deposition to target geometrically static air-water interfaces with polymer microspheres. In electrospray, a high electric potential is used to form a narrow liquid jet (diameter ~10 μm) at the outlet of an emitter, which breaks up into a plume of microdroplets containing the suspended material. Electrospray is an advantageous method for delivering particles to an interface, as the volatile solvent containing the particles fully evaporates in flight, minimizing initial disturbances at the interface. Furthermore, the accumulation and decay of electric charge on both the sprayed and surrounding materials has a significant impact on the deposition, whether the target is a solid or fluid.[30–32] Highly charged, insulative particles deposited to an interface will experience electrostatic repulsion, but the decay of this charge, particularly at the air-particle surface is still poorly understood. By creating a target substrate with a continuously replenished water supply, we can maintain a static interface shape and investigate the colloidal assembly dynamics for extended periods of time.

Both numerical and experimental studies have challenged traditional hydrodynamic theories on the motion of colloids at air-water interfaces.[33,34] However, there are a limited number of works which investigate the long-term behavior of colloidal particles at an interface. Bähler et.

al. observed a surprising interfacial rigidization over long time scales, and described various routes to reach an immobilized state.[35] To our knowledge, there are no studies which have used a field-driven process like electrospray to target an aqueous interface with microparticles and track the long-term evolution of the interfacial assembly of these highly charged colloids.

We seek to probe both the global colloidal assembly landscape, and the unexpected dissipative dynamics which arise when observing the air-water interface over long time scales. In Section 3.1, we report the results from experiments *with* NaCl added to the water subphase and discuss the particle assembly structure at different waiting times $t_w = t - t_0$, where t_0 represents the time that the spray was stopped. We show that structural ordering deteriorates over time ($t_w >$ 5 hours) due to electrostatic charge dissipation and conducted experiments to test our hypothesis using a single-point ionizer to "speed up" the charge dissipation process. Contrary to common wisdom, the addition of salt to the sub-phase improves hexagonal ordering of the interfacial particles. Section 3.2 discusses a more puzzling result when inspecting the particle motion at intermediate time scales ($t_w \sim 2$ hours). We observed a non-uniform transition of particle mobility, where neighboring particles have an order of magnitude difference in their diffusivity. UV-vis spectrometry revealed contaminants in the methanol/particle suspension, which would ultimately land on the interface and cause it to rigidify over time in a non-uniform manner.

2. Experimental Methods

2.1. Controllable Interface Platform

We designed a custom fluidic device to generate the controllable air-water interface. The device permitted the continuous infusion of water to balance evaporation and maintain a static interface. The interfacial curvature was monitored in real time with a machine-vision camera (Basler) and the infusion rate was modulated to fix the interface. The base substrate was FTO-coated glass (MSE PRO 2.2 mm 12-15 Ohm/Sq) with dimensions 25 mm × 75 mm × 2.2 mm. The manifold was 3D printed from PLA (Natural MatterHackers Build Series) on a Bambu Lab X1C with a 0.2 mm diameter stainless steel nozzle and is shown in **Figure S1**. Double-sided acrylic adhesive with a polyester backing tape was used to mount the manifold to the FTO coated glass surface. More details regarding the device assembly are provided in the Supplementary Information. The manifold carried the liquid subphase (de-ionized water or salt water) to an array of four holes, each with a diameter of either 1 mm or 2 mm. The water was held in a 3 mL syringe, which was loaded into a syringe pump (Chemyx Fusion 200) and connected to the manifold with

poly(tetrafluoroethylene) (PTFE) tubing. Liquid protruded from the holes in the manifold, forming well-defined spherical caps that remained pinned to the sharp edge of the opening. Images from the side-view camera were processed in real time (MATLAB) to fit a circular arc to the interface. The radius of curvature varied from 4 mm to 8 mm, which was necessary for detecting and controlling the interface shape and was too large to significantly impact the particle assembly. From the fit, we estimated the cap volume and the evaporation rate, and the syringe pump flow rate was set to hold the interface fixed. Given the slow evaporation kinetics of the air-water interface in ambient conditions, we only updated the flow rate every 1 to 2 seconds, which had a typical rate of around 0.5 μL/min.

2.2. Colloidal Suspension and Interfacial Target Preparation

The suspension used for electrospray consisted of fluorescent polystyrene microparticles (Thermo Fisher Scientific, 468/508 nm excitation/emission) with a diameter of 2 μm dispersed in methanol (0.1 % v/v). Our previous work has shown that contaminants (e.g. surfactants) deposited by electrospray will accumulate at the interface, and lead to Marangoni flows due to a surface tension gradient.[36] To avoid this effect, we centrifuged the particles up to 5 times in DI water to minimize surfactant contamination. The target interface was generated with DI water having a resistivity of 18 MΩ·cm. For some experiments, NaCl was added to the water before assembling the 3D printed manifold. We performed offline conductivity measurements of the water subphase to confirm that the salt concentration was accurate, using published values[37] to determine the mass concentration required to make the suspensions. For the DI water case, we inferred a salt concentration of 0.008 mM based on the measured conductivity. Since no salt was added, any source of conductivity was a result of environmental contamination.

2.3. Electrospray Deposition Procedure

Apart from the target substrate, the electrospray deposition setup was similar to our previous work.[32] Briefly, the colloidal suspension was delivered through PTFE tubing to a polyether ether ketone (PEEK) T-junction (IDEX) via a syringe pump (Chemyx). A short length of gold wire was used in the side port of the T-junction to connect the high voltage power supply (Spellman 230-20R). The electrospray occurred from a borosilicate glass capillary emitter in the T-junction, with a nominal inner diameter of 110 μm. The applied potential was ~3 kV, separation distance was 30 mm (measured from the emitter tip to the 3D printed manifold), and flow rate was 1.5 μL/min. These parameters, in conjunction with the dilute PS and methanol suspension, led to a stable cone-

jet spray regime. Across all experiments, the median temperature was 23.8 °C (IQR: 21.7–24.1 °C), and the median relative humidity was 23.7% (IQR: 16.8–33.3%). The particles adsorbed at the air-water interface were observed using an inverted microscope (Leica) on an optical table to minimize external disturbances. Monochrome images were captured with an EMCCD camera (Andor) at a maximum resolution of 1024 px × 1024 px. The spray was typically captured at 4 frames per second (fps), and the frame rate was reduced over time to avoid capturing redundant information. Notably, we increased the frame rate during some experiments to capture a shorter delay time, which is important for estimating the particle's diffusion coefficient as discussed in Section 3.2.

3. Results and Discussion

3.1. Role of Electrostatic Interactions in Colloidal Assembly Evolution

Our experimental setup is shown schematically in **Figure 1**. With the air-water interface held in a fixed position using our feedback control system, we targeted the substrate with PS particles. The grounded FTO layer was necessary for spray stability, and increases the efficiency of particle delivery to the target interface.[38] The spray duration varied across experiments but was typically 45 seconds – 1 minute to achieve a non-close packed interfacial density. After the spray was stopped, the full colloidal assembly reached a quasi-equilibrium state. The stabilizing force arises from the electrostatic charge imparted on the particles, but the exact location and behavior of this charge is not immediately apparent.

For an air-water system with micrometer scale particles, we expect electrostatic forces to dominate the assembly dynamics.[4] The electrostatic interaction energy far exceeds the thermal energy kT, so we anticipate long-range dipolar repulsion between particles to be the driving force, governed by a power law $F \propto 1/r^4$ where r is the equilibrium spacing.[39,40] The electric field responsible for this repulsion depends on the location of charges, i.e., either on the particle-air or particle-water surface. Methods have been developed to estimate which phase is primarily responsible for repulsion; typically, the electric field is much stronger in the air phase, especially when the electric double layer is thin relative to the particle radius.[41] However, the presence of dissolved ions in the water subphase can alter the charge landscape significantly, leading to screening of electrostatic repulsion. Collective, many-particle effects may also play a role in the assembly, as observed in both macro[42] and microscale[43] experiments. For example, the equilibrium

distance between particles could vary along the interface due to non-uniform displacement of the interface, but this effect was not seen in our work.

Figure 2 shows an assembly of particles evolving over a long duration (5.5 hours) for a 5 mM NaCl water subphase. A representative portion of the full interface with a region covering approximately 400 μm × 400 μm is shown to highlight qualitative differences in the assembly over time. The progression of **Figure 2a** to **Figure 2d** displays the transition of the interfacial assembly from a stable, partially ordered regime to a disordered, aggregated state. A full timelapse of the interfacial evolution is provided in Video S1. In **Figure 2a**, the particles are well-separated, consistent with strong electrostatic repulsion, with a few aggregates that likely formed before being deposited to the interface. The assembly appears similar after $t_w = 30$ min, but clearly loses some ordering after $t_w > 2$ hr as shown in **Figure 2b** and **c**, respectively. Finally, after $t_w > 5$ hr, the initial configuration is unrecognizable.

Particle ordering as a function of time is quantified in **Figure 3** and indicates progressively weaker interparticle repulsion. First, in **Figure 3a** we plot the sixfold orientation order parameter for each particle, calculated as $\psi_6 = \left|\frac{1}{N_j}\sum_j \exp 6\theta_j i\right|$ where we take the magnitude of the average value of the complex-valued function $\exp 6\theta_j i$ to estimate the local ordering. Here, θ_j represents the angle formed between a reference axis and a line connecting the particle of interest to its j-th neighbor. For ideal hexagonal ordering with $\theta_j = \frac{\pi}{3}$ rad we have $\psi_6 = 1$, whereas $\psi_6 = 0$ corresponds to complete disorder. Notably, we observe a decrease in the ensemble-averaged order parameter from $\langle\psi_6\rangle = 0.49$ at $t_w = 2$ min to $\langle\psi_6\rangle = 0.40$ at $t_w = 330$ min $= 5.5$ hr. This difference highlights the loss of hexagonal ordering of the interfacial particle assembly over time. Beyond the global reduction in $\langle\psi_6\rangle$, the distribution of ψ_6 values also shifts with increasing t_w, particularly in the upper range. For instance, 26.1% of particles at $t_w = 2$ min fall between $0.75 \leq \psi_6 \leq 1$, while only 4.8% of particles fall in this range at $t_w = 330$ min as shown in **Figure S2**.

The radial distribution function of the particles at the varying waiting times is shown in **Figure 3b**. The magnitude of the peaks decreases monotonically with t_w, providing additional evidence of reduced hexagonal ordering with time. Interestingly, the position of the first peak (corresponding to the primary equilibrium distance) initially shifts left, indicating a reduction in the average spacing between particles and therefore lower interparticle repulsion. Then, the peak shifts back to the right, closer to the original spacing $r = 10.4$ μm as shown in **Figure 3b** for $t_w =$

2 min. This shift can be attributed to particle aggregation; once aggregates form, they are detected as a single particle in our image processing pipeline which effectively increases the calculated equilibrium distance. When compared to the findings of Kralchevsky et al., our results are consistent with a reduction in charge at the particle-air surface from $t_w = 2$ min to $t_w = 330$ min.[4,41] Aggregates should function as larger, highly charged units resulting in a stronger overall electrostatic repulsion in the monolayer, with a higher average separation distance. However, the spacing is slightly less at $t_w = 330$ min, so the repulsive electrostatic force must be reduced.

We believe that the loss in hexagonal ordering over time can be attributed to the decay of electrostatic charge on the particle-air surface, for the 5 mM NaCl water subphase. The exact mechanism by which charge dissipates is elusive, but it is well known that static surface charge dissipates in ambient conditions due to moisture in the air, i.e. humidity.[44] The rate of decay in macroscopic environments is highly dependent on the relative humidity (RH); notably, we did not observe a meaningful change in the time scale of dissipation between experiments with a minimum average RH of 18% and maximum of 56%. However, considering the continuous evaporation and replenishment of water while the particles are located directly at the air-water interface, the local RH in the vicinity of the particle-air surface may be consistent across experiments, regardless of the ambient humidity.

The evolution of the interfacial assembly indicates that the decay of charge on the air side of the particles dominates their dynamics. To further probe this effect, we used a single-point ionizer (Simco-Ion) to neutralize static charge in the vicinity of the interface (**Figure 4**). The results show a fast rearrangement of the particle assembly after the ion source is enabled for at least 3 seconds. With the same 5 mM salt subphase and general electrospray procedure, the ionizer was placed 50 mm from the target, which minimized the disturbance to the interface, as shown in Video S2. At a separation of 20 mm, the particles were significantly disturbed, likely due to the "ionic wind" effect. To quantify the aggregation dynamics, we tracked the particle motion and estimated the proportion of single particles to aggregates. As shown in **Figure S3**, the number of detected particles falls sharply at $t_e = 20$ s, corresponding to 3 seconds of cumulative ion source activation time. This drop is indicative of aggregation, as particles merge and are detected as a single spot; however, particle detections alone cannot capture the proportion of remaining single particles to aggregates. Therefore, we use the number of track merging events to resolve the distribution of

aggregates. Tracks containing a single particle will have zero merges, while one merge = two particles, two merges = three particles, and so on. This relationship for the aggregate size $n_{\mathrm{agg}} = n_{\mathrm{merges}} + 1$ was used to create the histogram in **Figure S3**. About 40 seconds after the ion source was activated, the proportion of aggregates increased from < 1% to 43%.

The rapid aggregation of particles upon activation of the external ion source demonstrates that electrostatic charge decay on the air side of the particles reduces the repulsive dipolar forces that initially maintain particle separation. Furthermore, when comparing the particle assembly in t_2 from **Figure 4** to the assembly in **Figure 2d**, there are qualitative similarities of a disordered, partially aggregated regime, suggesting an environment with similar interparticle forces. A quantitative comparison of the structure before and after ionization is provided at the end of section 3.1. Note that it has been shown that non-uniform wetting of particles can induce an attractive, long range force between colloids at an interface.[45] Although we cannot estimate any heterogeneity of the triple contact line in our experiments, we acknowledge that an attractive force may be present due to this effect. Ultimately, we maintain that the dissipation of electric charge on the air side of the particles is the most significant factor in the long-term behavior, and any attractive force between particles only plays a role when the particle-air charge is reduced.

These observations underscore the dominant role of charge in the air phase and its role in driving interfacial aggregation; however, interparticle interactions can also be modulated by changes in electrostatic screening within the liquid subphase. To isolate the relative contribution of ionic strength in the water subphase, we conducted a separate set of experiments varying NaCl concentration while keeping all other parameters fixed. Previous works have found that the addition of salt to the aqueous phase can *disrupt* hexagonal ordering of interfacial colloids due to screening of electrostatic repulsion in the non-polar phase.[46,47] Here, we observe a much different behavior with electrosprayed particles introduced from the air phase. As shown in **Figure 5**, DI water exhibits lower hexagonal ordering for low t_w, compared to the 1 and 5 mM NaCl cases. Again, we highlight the sixfold orientation ordering parameter to quantify differences in the assembly structures. The 5 mM NaCl case has the highest value for $\langle\psi_6\rangle$, while the 0 mM case (DI water) has the lowest $\langle\psi_6\rangle$. The key difference between our results and studies from other authors arises from the delivery of the particles. When targeting the air-water interface with particles via electrospray, charge is imparted on the particles, but also on the interface itself. In a low electrolyte environment, this charge can accumulate, and screen repulsion through the air. A similar effect

was observed in our previous experiments targeting sessile droplets of trimethylolpropane ethoxylate triacrylate (ETPTA), a non-volatile liquid with low electrical conductivity. Crucially, this is a result of charge in the air phase, not in the water as is typically the case in Langmuir–Blodgett trough experiments. With salt added to the water, charge at the interface can be neutralized, and the dipolar repulsion between particles governs the assembly.

This effect is shown schematically in **Figure 6**. In the absence of salt (**Figure 6a**), positive ions from the electrospray accumulate at the air-water interface, forming a static charge layer. This occurs because deionized water has insufficient mobile charge carriers to neutralize incoming ions. The surface charge can locally immobilize the interface heterogeneously, leading to disordered, non-uniform particle spacing.[48] When salt is added to the water (**Figure 6b**), mobile ions (primarily Cl^-) diffuse toward the interface and neutralize the surface charge from the electrospray. The dipolar repulsion $F \propto 1/r^4$ provides an isotropic, repulsive force leading to partial hexagonal ordering. Simultaneously, a "depletion region" forms, consistent with our previous work and indicative of strong electrostatic repulsion between the surrounding substrate and interfacial particles. However, our previous experiments targeting sessile droplets on a solid substrate exhibited minimal changes in ordering when salt was added to the water.[32] The key difference lies in the geometry: the 1 mm deep water reservoir in the present work is 20× taller than the 50 μm photoresist "step" used to define sessile droplet shapes. We believe this change in thickness is causing the DI water case to repeatedly achieve worse hexagonal ordering than the 5 mM salt case, as the taller substrate geometry increases the diffusion time of trace ions to the interface. Considering the 0 mM case as a baseline, the increase in hexagonal ordering as indicated by ψ_6 is roughly proportional to the ionic strength increase.

Finally, we introduce the Voronoi entropy as an additional method to quantify structural changes at the interface over time, which has been used as a metric to evaluate global ordering behavior in colloidal systems.[49,50] A Voronoi diagram is constructed from our particle positions at multiple t_w, which forms polygonal cells defining the set of points closest to a given particle. Then, the Voronoi entropy is calculated as $S_{\mathrm{vor}} = -\sum_{i=3}^{n} p_i \ln p_i$ where p_i is the fraction of polygons with i sides. Lower S_{vor} values correspond to a more ordered structure, e.g., a perfect hexagonal lattice will have a Voronoi diagram with hexagonal cells only, excluding the boundaries. As $p_6 \to 1$, $\ln p_6 \to 0$, while $p_{i\neq 6} \to 0$, driving the sum to zero. This is in contrast to ψ_6, for which lower values correspond to less hexagonal ordering, with $\psi_6 = 1$ in the ideal hexagonal lattice.

In **Figure 7**, we compare the Voronoi entropy to the ensemble-averaged sixfold orientation order parameter $\langle\psi_6\rangle$ for the DI water and 5 mM salt cases. In both cases, the metrics are inversely correlated: Voronoi entropy increases over time while $\langle\psi_6\rangle$ decreases, as indicated by the Pearson correlation coefficient for the DI water sample $(r_{xy} = -0.927)$ and the 5 mM salt sample $(r_{xy} = -0.964)$. Notably, the Voronoi entropy is initially higher for DI water, which relates to the preceding paragraph regarding the lack of mobile charge carriers. A continuous measure of symmetry (CSM) was also calculated and found to be highly correlated with S_{vor}, more details are provided in **Figure S4** of the Supplementary Information.[51]

Collectively, these metrics point to increasing disorder of the PS particle assembly over time. Connecting the long-term DI water and 5 mM salt results to the ion source experiment, **Figure 7** also shows the Voronoi entropy and $\langle\psi_6\rangle$ parameter before and after neutralization. Before neutralization (square markers), the metrics resemble the 5 mM case; after neutralization (six-pointed star markers), they align with the DI water case which consistently had a higher Voronoi entropy and lower $\langle\psi_6\rangle$ until longer t_w. This demonstrates that a more disordered assembly can be directly caused by electrostatic charge neutralization, and the same outcome can be reached by simply waiting for longer t_w. Furthermore, this captures the necessity of mobile charge carriers in the water to neutralize charge at the interface and enable some degree of hexagonal ordering when depositing colloidal particles via electrospray.

By analyzing the long-term evolution of the interface and elucidating the role of electrolyte concentration, we have shown the significance of electrostatic charge in our experiments, in both the air and water phases. Electrospray imparts charge on the particles and other surfaces near the target substrate, including the interface itself. While the initial configuration of the particles is influenced by the electrolyte concentration in the subphase, over long time scales (> 5 hours) any hexagonal ordering due to isotropic repulsion is lost, as the charge on the particle-air surface dissipates.

3.2. Anomalous Diffusion at Intermediate Time Scales

At intermediate time scales, e.g. $t_w = 1.5$ hours, we observed an unexpected phenomenon where the diffusivity of the particles varied by at least an order of magnitude, as shown in Video S3. Some particles appear to be moving randomly due to thermal fluctuations, while other particles, in many cases direct neighbors to those mobile ones, appear to be completely fixed in place. We tracked particles and calculated the mean-squared displacement (MSD) to elucidate the

particle diffusion characteristics, as shown in **Figure 8**. More details about the particle tracking and MSD calculation are provided in the Supplementary Information; the TrackMate plugin in Fiji was used extensively to detect and track the PS particles at the interface.[52] The particles fall into one of two groups, which we label as "low" and "high" mobility on the figure. At short delay times $\tau < 1$ s, the high mobility particles have an average MSD curve with a slope near 1, indicative of pure Brownian motion. This curve flattens out over time, as caging due to neighbors leads to a sub-diffusive regime.[20] Notably, the diffusion constant $D_{\text{high}} = 0.146\ \mu\text{m}^2/\text{s}$ is equal to 0.74 times the diffusion coefficient of the same particle immersed in water: $D_{\text{bulk}} = 0.215\ \mu\text{m}^2/\text{s}$ calculated using the Stokes-Einstein relationship $D = \frac{kT}{6\pi\eta R}$ where $\eta = 10^{-3}$ Pa · s is the dynamic viscosity of water and $R = 1 \times 10^{-6}$ m is the particle radius. That is, particles at the interface have a *lower* diffusivity, even though a portion of the particle is immersed in a much lower viscosity medium, air. This agrees remarkably well with the results of Boniello et. al.[33], who found that the translational viscous drag at the interface was *higher* than viscous drag in the bulk. This is equivalent to our result framed in terms of the diffusion constant, as the translation viscous drag $\gamma_T = \frac{kT}{D}$ is inversely proportional to D.

While this experimental agreement is promising, the "low" mobility particles require further consideration. These particles appear to be completely immobilized, while their neighbors diffuse around within a caged region. First, the MSD does not have a slope of 1 even at early delay times, indicative of sub-diffusive behavior. Therefore, these particles are not undergoing detectable Brownian motion and their ability to diffuse freely is significantly inhibited. The Stokes-Einstein equation holds for small (non-inertial) particles immersed in a Newtonian solvent.[53] If the high-mobility particles are governed by the viscous response of the air-water interface, the low-mobility particles may be influenced by a viscoelastic force. A potential source of viscoelasticity at an interface could be contamination of organic molecules, e.g. polymers or surfactants. We considered measuring the interfacial tension of the water to probe for surfactant contamination; however, there would be no practical method to measure the surface tension in-situ. Instead, our approach was to analyze the electrospray suspension to search for contaminants.

Following a method similar to Bähler et. al.[35], we performed UV-vis spectrometry on the methanol/PS particle suspension. We show the spectrometry results in **Figure 9**, which plot the absorbance of our electrospray suspension supernatant relative to pure methanol. We also show

the absorbance spectrum of a polystyrene reference material, PS1300, which was dispersed in the same methanol solvent. Following the procedure described in Section 2.2, the PS 2 μm and PS1300 supernatants were generated by allowing the polystyrene to sit in the methanol for 1 week to simulate the time between suspension preparation and spraying. Then, the particles were centrifuged to extract the methanol supernatant for each suspension. We measured the transmission of light across a broad UV-vis range with $T = I/I_0$ where I was the intensity of light passing through the supernatant, and I_0 was the intensity of light passing through the HPLC-grade methanol solvent. The absorbance was calculated as $A = \log_{10}\frac{1}{T}$ and was normalized to the maximum absorbance value, as we were only interested in the relative position of absorbance peaks. When comparing the PS 2 μm and PS1300 spectra, we see a close match at 225 nm, with the PS1300 showing a second peak around 260 nm. Furthermore, the PS 2 μm has a non-negligible absorbance signal around 450 nm, which is close the 468 nm excitation wavelength of the fluorophore embedded in the particles. While this implies that some fluorophores were detached from the PS particles, the relative signal is very weak compared to the UV absorbance. The closely matched UV peak shows that there are likely short-chain polystyrene molecules present in the spray suspension, which are inevitably delivered to the interface.

If the immobilization of particles is caused by contaminants, more details are required to explain why the particle-to-particle diffusion is anisotropic. Importantly, the experimental results of Bähler et. al. show a *homogenous* immobilization over a 24-hour period, where the non-close packed and ordered structure of the interface was maintained. This may be attributed to the use of decane as the non-polar fluid, which limits charge dissipation compared to the particle-air surface. To be clear, this does not show that higher charge itself causes immobilization, it simply maintains the ordering on a longer time scale than the rigidification. Park et. al. saw some variation in the pair interaction between particles at a decane-water interface; however, the difference was only up to a factor of two.[54] Although we do not measure the pair potential here, the diffusivity varies by up to a factor of 10, which is unlikely a result of charge inhomogeneity on the particles alone. We contend that the variation of particle mobility among direct neighbors is due to heterogeneity in the contaminants which are present at the interface. Furthermore, the origin of this heterogeneity may arise from differences in the contact angle at the particle surface, as shown diagrammatically in **Figure 10**. A particle protruding out of the water phase ($\theta > 90°$, **Figure 10b**) will locally inhibit evaporation near the contact line.[55] This varying evaporative flux will necessarily create a

weak flow field at the interface, which is directed radially outward from the particle and effectively repels the organic contaminants. Meanwhile, particles more immersed in water ($\theta < 90°$, **Figure 10c**) will experience the opposite effect and attract contaminants. Our justification for the non-equilibrium or "perturbed" state of particle wetting arises from a recent study, which showed that colloids can take hours to reach an equilibrium contact angle at an interface.[56] At intermediate time scales, particles may experience different degrees of rigidification due to the long relaxation time of the contact angle, but ultimately, after long periods of time (> 6 hours), the interface becomes fully rigidified as shown in **Figure 2d**.

The contact angle variation may be caused by differences in the particle velocity as it travels from the electrospray emitter to the interface. We can obtain a first order estimate for the terminal velocity of a particle deposited via electrospray by considering the balance of electrostatic and drag forces. For a spherical particle, we have the Stoke's drag $F_d = 6\pi\eta r v$ and electrostatic force $F_e = qE$. Setting these equal, we find $v_t = \frac{qV}{6\pi\eta r d}$ where we assume a uniform field, $E = V/d$. Therefore, the terminal velocity of a particle is directly proportional to its charge $v_t \propto q$ and the electric field strength $v_t \propto \frac{V}{d}$. The field strength in the electrospray plume should be uniform, but the charge of individual particles can vary significantly, depending on the size of the solvent droplet encapsulating it. In the jet breakup process, larger droplets undergoing evaporation will undergo Coulombic fission as they reach the Rayleigh limit, which is the theoretical maximum charge of a droplet.[57] The ejected solvent droplets will carry charge away, leaving the particle charge at a fraction of the Rayleigh limit. Meanwhile, smaller droplets may never reach the Rayleigh limit as they evaporate if the initial ratio $\frac{d_{\text{droplet}}}{d_{\text{particle}}}$ is low, leaving these particles with more charge. The actual variation in charge depends on many factors, but literature suggests that it can range from 20% - 80%, meaning the velocity would vary by up to a factor of four.[58] Ultimately, this variation in charge, and therefore velocity, may lead to a heterogeneous distribution of contact angles, which causes contaminants at the interface to accumulate around the particles at different rates.

4. Conclusion

In this work, we delivered insulative microparticles to a static air-water interface using electrospray deposition. By eliminating the flow-driven effects of evaporation, we were able to uncover previously unseen interfacial phenomena over extended timescales. We found that electrostatic charge dissipation on the air side of the particles plays a central role in the time-dependent aggregation of particles. Furthermore, the neutralization of surface charge via an ion source confirmed the dominance of electrostatic forces in the air phase, effectively eliminating any ordering between the interfacial particles. These observations are consistent with prior studies describing soft electrostatic repulsion in monolayers and the importance of mobile charges at fluid interfaces.[4,41,48] The effect of electrolyte concentration in the water subphase was considered, as adding a salt such as NaCl was necessary to achieve measurable hexagonal ordering in our system. This was unexpected given the findings from our previous work and other authors but could be justified considering the unique process of electrospray and modifications to the target substrate.[32,54,59]

At intermediate time scales, we observed heterogeneity in particle mobility, where some particles diffused freely while others were nearly immobile. By tracking the particles with sufficient temporal resolution, we found that the more mobile particles had a reasonable diffusivity value, consistent with recent work considering polymeric particles at an air-water interface.[33,34] Meanwhile, the less mobile particles appeared rigidified, and over the course of hours, all particles reached this immobilized state. To our knowledge, this heterogenous diffusion behavior has not been observed or analyzed in interfacial colloidal systems. By investigating the composition of the electrospray suspension, we found that polystyrene oligomers may be present in the methanol solvent and could inhibit diffusion of colloids at the interface.[35] The neighbor-to-neighbor discrepancy of diffusion was likely caused by contact angle variation and slow relaxation, leading to non-uniform accumulation of contaminants around the particles.[56] Electrospray targeting combined with long-term observation offers a useful tool for studying nonequilibrium colloidal assembly and mobility transitions not accessible in equilibrium systems. Extending our approach to include contact angle measurements during or immediately after deposition could help uncover how local wetting transitions contribute to particle immobilization.

Supplementary Information

- Fluidic device assembly and local drift velocity correction method (.pdf)
- Video of assembly evolution over 21 hours (.mp4)
- Video of ionizer experiment (.mp4)
- Video of anomalous diffusion of particles (.mp4)

Data Availability

Data for this article are available at the following GitHub repository: https://github.com/Chiarot-Lab/electrospray-evolution-interface

Acknowledgements

The authors gratefully acknowledge the support of the National Science Foundation Advanced Manufacturing program through Awards 1939362 and 2400546.

Declaration of generative AI and AI-assisted technologies in the writing process

During the preparation of this work, the authors used OpenAI's ChatGPT (model 4o) in order to suggest minor revisions to the language and flow. After using this service, the authors reviewed and edited the content as needed and take full responsibility for the content of the published article.

References

1. Wilts, B. D. *et al.* Butterfly gyroid nanostructures as a time-frozen glimpse of intracellular membrane development. *Science Advances* **3**, e1603119 (2017).
2. Borah, R., Ag, K. R., Minja, A. C. & Verbruggen, S. W. A Review on Self-Assembly of Colloidal Nanoparticles into Clusters, Patterns, and Films: Emerging Synthesis Techniques and Applications. *Small Methods* **7**, 2201536 (2023).
3. Vialetto, J. & Anyfantakis, M. Exploiting Additives for Directing the Adsorption and Organization of Colloid Particles at Fluid Interfaces. *Langmuir* **37**, 9302–9335 (2021).
4. Kralchevsky, P. A., Danov, K. D. & Petkov, P. V. Soft electrostatic repulsion in particle monolayers at liquid interfaces: Surface pressure and effect of aggregation. *Philosophical Transactions of the Royal Society A: Mathematical, Physical and Engineering Sciences* **374**, (2016).
5. Pieranski, P. Two-Dimensional Interfacial Colloidal Crystals. *Physical Review Letters* **45**, 569–572 (1980).
6. Wang, D. *et al.* Quantitative 3D real-space analysis of Laves phase supraparticles. *Nat Commun* **12**, 3980 (2021).

7. Maestro, A. & Guzmán, E. Colloids at Fluid Interfaces. *Processes* **7**, 942 (2019).
8. Anyfantakis, M. *et al.* Adsorption and Crystallization of Particles at the Air-Water Interface Induced by Minute Amounts of Surfactant. *Langmuir* **34**, 15526–15536 (2018).
9. Liljeström, V., Chen, C., Dommersnes, P., Fossum, J. O. & Gröschel, A. H. Active structuring of colloids through field-driven self-assembly. *Current Opinion in Colloid & Interface Science* **40**, 25–41 (2019).
10. Anjali, T. G. & Basavaraj, M. G. Shape-induced deformation, capillary bridging, and self-assembly of cuboids at the fluid-fluid interface. *Langmuir* **33**, 791–801 (2017).
11. Danov, K. D., Kralchevsky, P. A., Naydenov, B. N. & Brenn, G. Interactions between particles with an undulated contact line at a fluid interface: Capillary multipoles of arbitrary order. *Journal of Colloid and Interface Science* **287**, 121–134 (2005).
12. Trevenen, S. *et al.* Nanoscale Porosity in Microellipsoids Cloaks Interparticle Capillary Attraction at Fluid Interfaces. *ACS Nano* **17**, 11892–11904 (2023).
13. Solano-Cabrera, C. O. *et al.* Self-Assembly and Transport Phenomena of Colloids: Confinement and Geometrical Effects. *Annual Review of Condensed Matter Physics* **16**, 41–59 (2025).
14. Kim, P. Y., Dinsmore, A. D., Hoagland, D. A. & Russell, T. P. Wetting, meniscus structure, and capillary interactions of microspheres bound to a cylindrical liquid interface. *Soft Matter* **14**, 2131–2141 (2018).
15. Ershov, D., Sprakel, J., Appel, J., Cohen Stuart, M. A. & van der Gucht, J. Capillarity-induced ordering of spherical colloids on an interface with anisotropic curvature. *Proceedings of the National Academy of Sciences* **110**, 9220–9224 (2013).
16. Williams, D. F. & Berg, J. C. The aggregation of colloidal particles at the air—water interface. *Journal of Colloid and Interface Science* **152**, 218–229 (1992).
17. Abdel-Fattah, A. I. & El-Genk, M. S. Sorption of Hydrophobic, Negatively Charged Microspheres onto a Stagnant Air/Water Interface. *Journal of Colloid and Interface Science* **202**, 417–429 (1998).
18. Aveyard, R. *et al.* Measurement of long-range repulsive forces between charged particles at an oil-water interface. *Physical Review Letters* **88**, 2461021–2461024 (2002).
19. Horozov, T. S., Aveyard, R., Clint, J. H. & Binks, B. P. Order-disorder transition in monolayers of modified monodisperse silica particles at the octane-water interface. *Langmuir* **19**, 2822–2829 (2003).
20. Parolini, L., Law, A. D., Maestro, A., Buzza, D. M. A. & Cicuta, P. Interaction between colloidal particles on an oil–water interface in dilute and dense phases. *Journal of Physics: Condensed Matter* **27**, 194119 (2015).
21. Zhao, M. & Yong, X. Nanoparticle motion on the surface of drying droplets. *Physical Review Fluids* **3**, (2018).
22. Bigioni, T. P. *et al.* Kinetically driven self assembly of highly ordered nanoparticle monolayers. *Nature Materials* **5**, 265–270 (2006).
23. Amiri, N., Prisaznuk, J. M., Huang, P., Chiarot, P. R. & Yong, X. Deep-learning-enhanced modeling of electrosprayed particle assembly on non-spherical droplet surfaces. *Soft Matter* https://doi.org/10.1039/D4SM01160K (2025) doi:10.1039/D4SM01160K.
24. Al-Milaji, K. N., Secondo, R. R., Ng, T. N., Kinsey, N. & Zhao, H. Interfacial Self-Assembly of Colloidal Nanoparticles in Dual-Droplet Inkjet Printing. *Advanced Materials Interfaces* **5**, 1–11 (2018).

25. Li, Y., Yang, Q., Li, M. & Song, Y. Rate-dependent interface capture beyond the coffee-ring effect. *Sci Rep* **6**, 24628 (2016).
26. Hu, H. & G. Larson, R. Analysis of the Effects of Marangoni Stresses on the Microflow in an Evaporating Sessile Droplet. *Langmuir* **21**, 3972–3980 (2005).
27. Sauleda, M. L., Chu, H. C. W., Tilton, R. D. & Garoff, S. Surfactant Driven Marangoni Spreading in the Presence of Predeposited Insoluble Surfactant Monolayers. *Langmuir* **37**, 3309–3320 (2021).
28. Fernández-Toledano, J. C., Moncho-Jordá, A., Martínez-López, F. & Hidalgo-Álvarez, R. Spontaneous formation of mesostructures in colloidal monolayers trapped at the air-water interface: A simple explanation. *Langmuir* **20**, 6977–6980 (2004).
29. Roger, K., Liebi, M., Heimdal, J., Pham, Q. D. & Sparr, E. Controlling water evaporation through self-assembly. *Proceedings of the National Academy of Sciences* **113**, 10275–10280 (2016).
30. Kingsley, B. J. & Chiarot, P. R. Polyimide Films Manufactured Using Partially Wet Electrospray Deposition. *ACS Applied Polymer Materials* https://doi.org/10.1021/acsapm.2c01891 (2023) doi:10.1021/acsapm.2c01891.
31. Lei, L. *et al.* Self-limiting electrospray deposition on polymer templates. *Scientific Reports* **10**, 1–9 (2020).
32. Prisaznuk, J. M., Huang, P., Yong, X. & Chiarot, P. R. Probing Colloidal Assembly on Non-Axisymmetric Droplet Surfaces via Electrospray. *Langmuir* **39**, 469–477 (2023).
33. Boniello, G. *et al.* Brownian diffusion of a partially wetted colloid. *Nature Materials* **14**, 908–911 (2015).
34. Villa, S., Boniello, G., Stocco, A. & Nobili, M. Motion of micro- and nano- particles interacting with a fluid interface. *Advances in Colloid and Interface Science* **284**, 102262 (2020).
35. Bähler, P., Zanini, M., Morgese, G., Benetti, E. & Isa, L. Immobilization of Colloidal Monolayers at Fluid–Fluid Interfaces. *Gels* **2**, 19 (2016).
36. Ghafouri, A., Zhao, M., Singler, T. J., Yong, X. & Chiarot, P. R. Interfacial Targeting of Sessile Droplets Using Electrospray. *Langmuir* **34**, 7445–7454 (2018).
37. Quan, X. *et al.* Capacitive deionization of NaCl solutions with ambient pressure dried carbon aerogel microsphere electrodes. *RSC Adv.* **7**, 35875–35882 (2017).
38. Park, S. H. *et al.* Efficient electrospray deposition of surfaces smaller than the spray plume. *Nature Communications* **14**, 4896 (2023).
39. Hurd, A. J. The electrostatic interaction between interfacial colloidal particles. *Journal of Physics A: Mathematical and General* **18**, L1055–L1060 (1985).
40. Paunov, Vesselin. N. Electrostatic interaction between charged colloid particles entrapped in a thin electrolyte film: confinement effects. *Colloid Polym Sci* **281**, 701–707 (2003).
41. Petkov, P. V., Danov, K. D. & Kralchevsky, P. A. Surface Pressure Isotherm for a Monolayer of Charged Colloidal Particles at a Water/Nonpolar-Fluid Interface: Experiment and Theoretical Model. *Langmuir* **30**, 2768–2778 (2014).
42. Vandewalle, N., Obara, N. & Lumay, G. Mesoscale structures from magnetocapillary self-assembly. *The European Physical Journal E* **36**, 127 (2013).
43. Lee, D.-G., Cicuta, P. & Vella, D. Self-assembly of repulsive interfacial particles via collective sinking. *Soft Matter* **13**, 212–221 (2017).

44. Cardenas, Z. *et al.* Effect of Humidity on Charge Decay in Varying Atmospheric Gases. in *2021 IEEE Pulsed Power Conference (PPC)* 1–5 (2021). doi:10.1109/PPC40517.2021.9733134.
45. Jun Park, B. & M. Furst, E. Attractive interactions between colloids at the oil–water interface. *Soft Matter* **7**, 7676–7682 (2011).
46. Aveyard, R., Clint, J. H., Nees, D. & Paunov, V. N. Compression and structure of monolayers of charged latex particles at air/water and octane/water interfaces. *Langmuir* **16**, 1969–1979 (2000).
47. Petkov, P. V., Danov, K. D. & Kralchevsky, P. A. Monolayers of charged particles in a Langmuir trough: Could particle aggregation increase the surface pressure? *Journal of Colloid and Interface Science* **462**, 223–234 (2016).
48. Carnie, S. L., Del Castillo, L. & Horn, R. G. Mobile Surface Charge Can Immobilize the Air/Water Interface. *Langmuir* **35**, 16043–16052 (2019).
49. Frenkel, M. *et al.* Continuous Symmetry Measure vs Voronoi Entropy of Droplet Clusters. *J. Phys. Chem. C* **125**, 2431–2436 (2021).
50. Frenkel, M., Arya, P., Bormashenko, E. & Santer, S. Quantification of ordering in active light driven colloids. *Journal of Colloid and Interface Science* **586**, 866–875 (2021).
51. Zabrodsky, H., Peleg, S. & Avnir, D. Continuous symmetry measures. *J. Am. Chem. Soc.* **114**, 7843–7851 (1992).
52. Ershov, D. *et al.* TrackMate 7: integrating state-of-the-art segmentation algorithms into tracking pipelines. *Nat Methods* **19**, 829–832 (2022).
53. Zia, R. N. Active and Passive Microrheology: Theory and Simulation. *Annual Review of Fluid Mechanics* **50**, 371–405 (2018).
54. Park, B. J. *et al.* Direct Measurements of the Effects of Salt and Surfactant on Interaction Forces between Colloidal Particles at Water−Oil Interfaces. *Langmuir* **24**, 1686–1694 (2008).
55. Gelderblom, H., Diddens, C. & Marin, A. Evaporation-driven liquid flow in sessile droplets. *Soft Matter* **18**, 8535–8553 (2022).
56. Kaz, D. M., McGorty, R., Mani, M., Brenner, M. P. & Manoharan, V. N. Physical ageing of the contact line on colloidal particles at liquid interfaces. *Nature Materials* **11**, 138–142 (2012).
57. Grimm, R. L. & Beauchamp, J. L. Evaporation and Discharge Dynamics of Highly Charged Multicomponent Droplets Generated by Electrospray Ionization. *J. Phys. Chem. A* **114**, 1411–1419 (2010).
58. Gomez, A. & Tang, K. Charge and fission of droplets in electrostatic sprays. *Physics of Fluids* **6**, 404 (1998).
59. Nikolaides, M. G. *et al.* Electric-field-induced capillary attraction between like-charged particles at liquid interfaces. *Nature* **420**, 299–301 (2002).

Figures

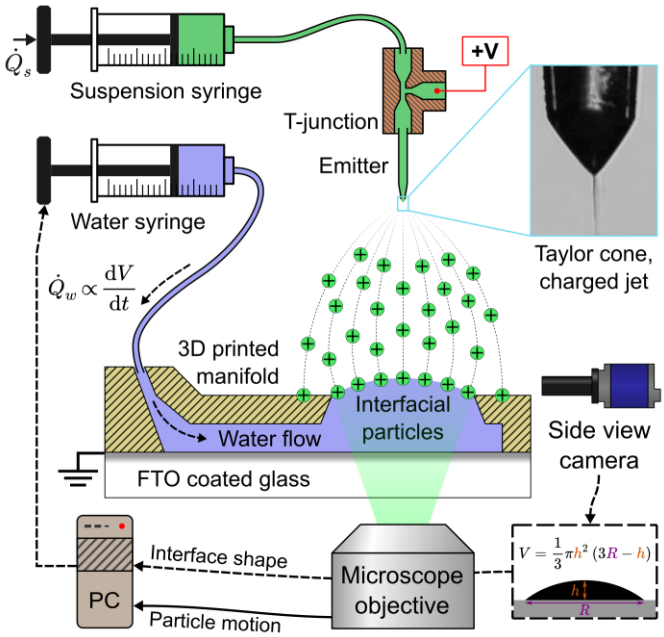

Figure 1. Experimental setup for in-situ interfacial particle delivery via electrospray. The steady air-water interface is generated by constantly infusing water through the 3D printed manifold. The electrospray is generated by a high voltage source, which is connected to a microfluidic emitter. A dilute suspension of polystyrene particles is delivered through the T-junction and glass emitter. At the tip of the emitter, a stable Taylor cone is formed as the surface tension of the suspension is balanced by the electrostatic field. The emitted jet subsequently breaks up and creates an atomized spray, delivering dry microparticles to the water air-interface below.

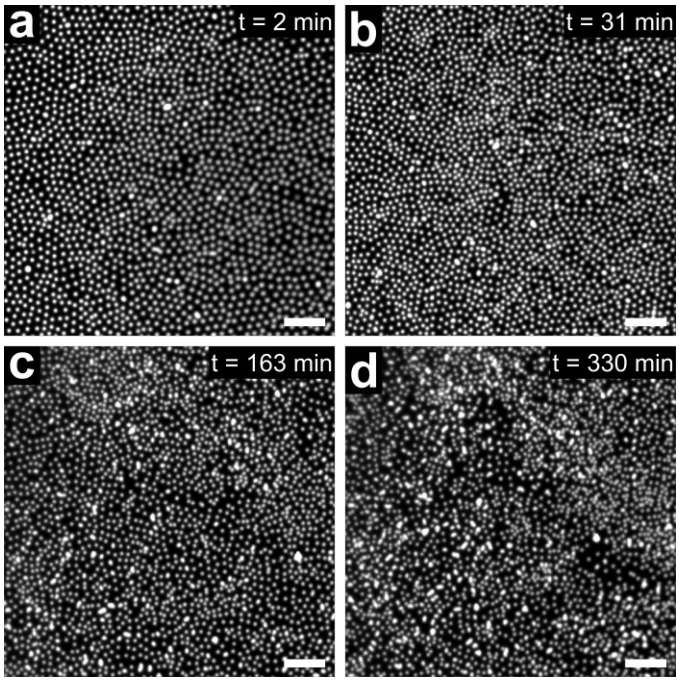

Figure 2. Microscope images of particle assembly at the air-water interface for increasing waiting times; the concentration of NaCl in the water was 5 mM for all cases. The initial assembly has regions of local hexagonal ordering, as individual particles have a well-defined primary separation distance. At short waiting times, the particles oscillate around their equilibrium position but globally remain fixed in the assembly due to caging from their neighbors. Over time, more aggregates appear as the interparticle repulsion begins to decline. Finally, after many hours the assembly is disordered, and random fluctuations in positions become undetectable in the full video. Scale bars for all panels are 50 μm.

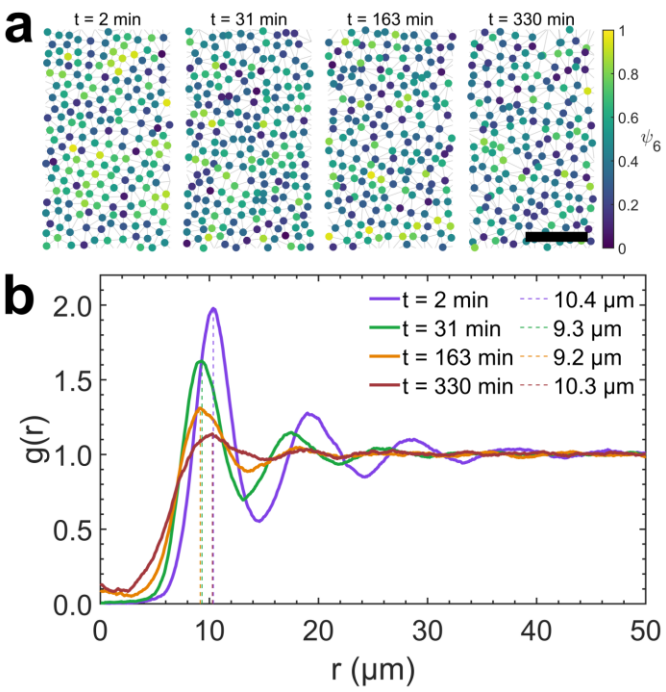

Figure 3. Particle ordering as a function of time. The sixfold orientational ordering parameter (a) is shown for a subregion of particles, whose position was extracted from microscope images. The average value for ψ_6 decreased monotonically as $\langle\psi_6\rangle = 0.49, 0.43, 0.43, 0.40$ for $t = 2, 31, 163, 330$ min, respectively. The radial distribution function (b) shows the evolution of the primary equilibrium distance between particles. Scale bar shown in (a) is 50 μm.

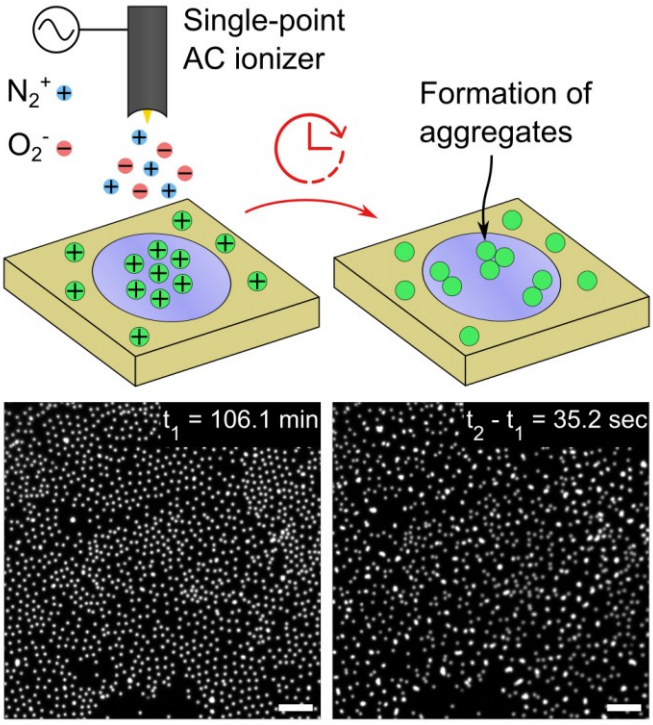

Figure 4. Single-point ionizer experiment. The schematic shows our ion source with a sharp metal tip and insulating body, which was connected to a high voltage AC source located 50 mm above the targeted interface. We enabled the AC source in 1 second increments until a notable change in the particle assembly structure was observed. The first image shows the time elapsed from the start of the experiment, t_w, just before the third activation of the ion source. The second image shows the aggregation of particles, about 30 seconds after the third and final neutralization was stopped. Scale bars are 50 μm.

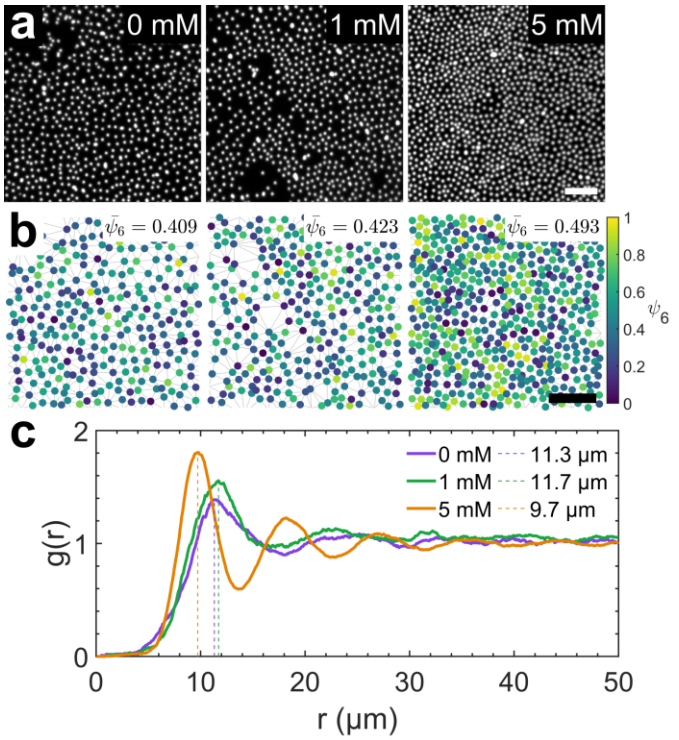

Figure 5. Particle assembly as a function of NaCl salt concentration. Microscope images (a) and extracted particle positions (b) are shown at $t_w = 5$ min for 0 and 1 mM NaCl, and $t_w = 10$ min for 5 mM NaCl. Scale bars shown in (a) and (b) are 50 μm.

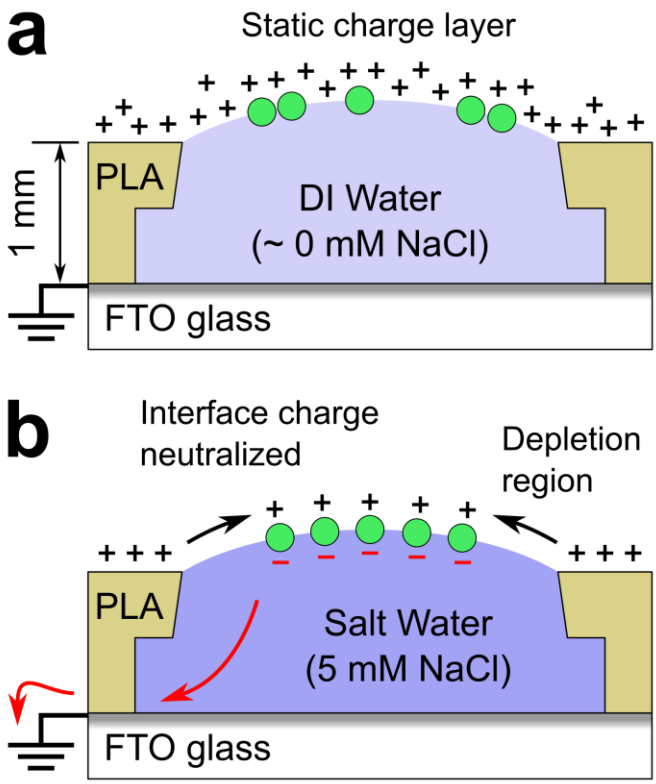

Figure 6. Schematic showing effect of adding salt to manifold. With no salt (a) the low ionic strength of the subphase allows a layer of positive electrostatic charge to accumulate at the air-water interface. The particles cover the entire interface and do not have consistent spacing between neighbors. With salt added to the water (b) there is more uniform spacing between particles, with a higher degree of hexagonal ordering. Additionally, particles are transported away from the insulative manifold via electrostatic repulsion, which is not observed for (a).

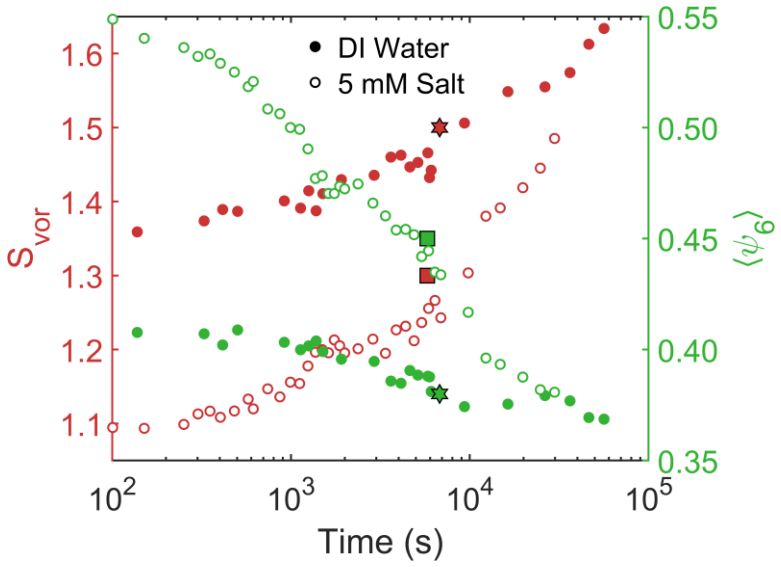

Figure 7. Time dependence of ordering parameters for DI water (filled circles) and 5 mM salt water (open circles). The left y-axis (red) shows the Voronoi entropy increasing over time. The right y-axis (green) shows the ensemble-averaged $\langle\psi_6\rangle$ parameter decreasing over time. The square and six-pointed star markers are overlaid from the ion neutralization experiment and indicate the value of the metrics before and after the ion source was applied, respectively.

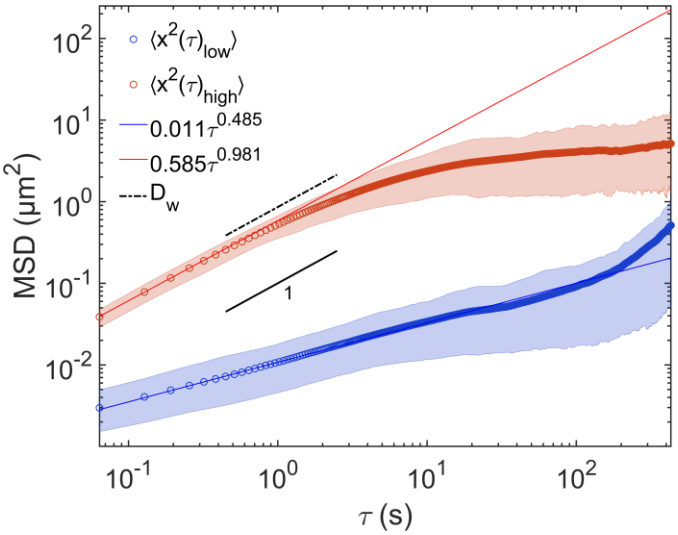

Figure 8. Mean-squared displacement of colloidal particles at an intermediate waiting time, $t_w = 1.5$ hr. The open circle markers represent the ensemble-averaged MSD, calculated with 70 particles for the upper curve, and 210 particles for the lower curve. Power-law fits for the lower and upper curves are shown with the blue and red lines, respectively, and were generated using short delay times $\tau < 0.5$ s. The bands represent the 10th and 90th percentile values of the MSD for each particle group. The solid black line with slope = 1 is included for reference, as well as the dot-dashed line representing the diffusivity of a similar particle fully immersed in water.

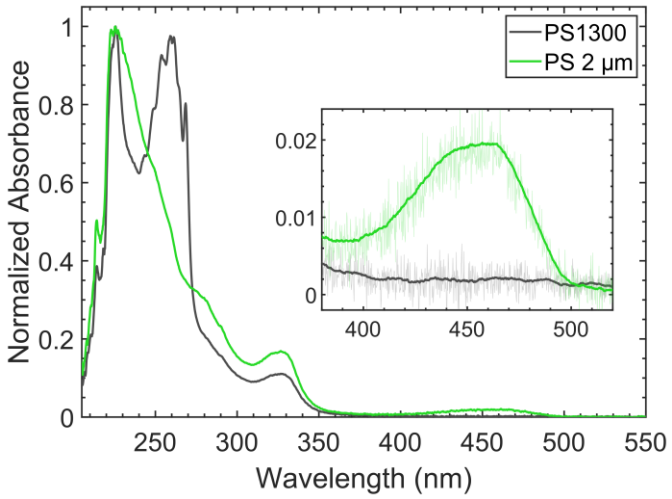

Figure 9. UV-vis spectra of two polystyrene supernatants. The PS1300 reference material supernatant is shown in gray and exhibits two local maxima at 225 and 260 nm. The PS 2 µm supernatant is shown in green and has a primary local maximum at 225 nm. The inset shows a region in the 400 to 500 nm range (visible blue light) where the PS 2 µm has a small, but detectable absorbance signal, while the PS1300 has essentially zero absorbance in this range.

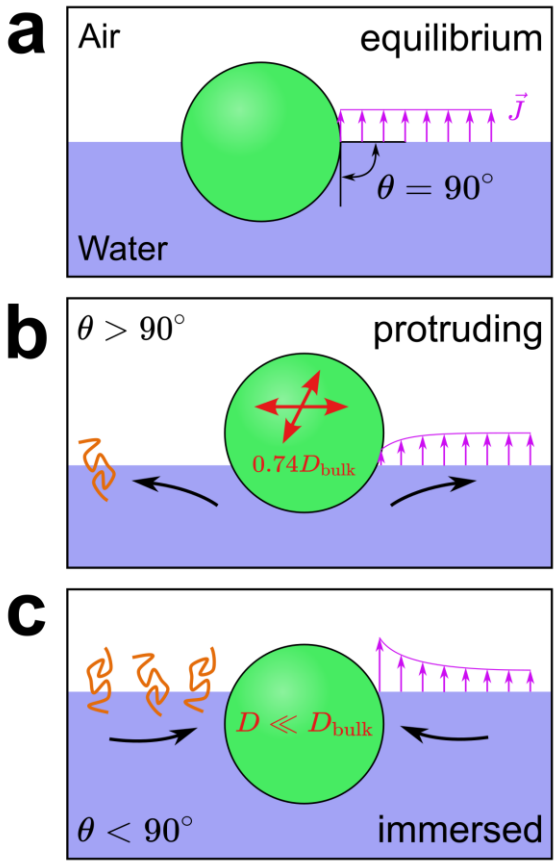

Figure 10. Proposed mechanism of non-uniform particle diffusion. A polystyrene particle in equilibrium at an air-water interface (a) has a contact angle near 90°. In (b) and (c), this particle is shown slightly protruding or immersed in the water, respectively. The interfacial diffusivity for (b), with contaminants not yet accumulated around the particle, is found to be less than the bulk diffusivity of a similar particle immersed in water. For (c), the organic contaminants (polystyrene oligomers) are shown in orange, and their accumulation rigidifies the interface locally. The contact angle discrepancy may be induced by variations in the impact velocity of the electrosprayed particles at the interface, leading to a non-uniform evaporative flux $\vec{J}$ and translational convection at the interface. Due to the slow relaxation of the contact line, contaminants at the interface have time to disperse from (b) or build up (c) at the particle surface, leading to highly local variations in the particle mobility.

Graphical Abstract